Flex-LCC: A New Grid-Forming HVDC Rectifier for Collecting Large-Scale Renewable Energy

Sun, Qianhao; Song, Qiang; Meng, Jingwei; Cui, Bin; Li, Gen; Cheng, Fan; Wang, Kailun

Published in:
IEEE Transactions on Industrial Electronics

Link to article, DOI:
10.1109/TIE.2023.3327527

Publication date:
2024

Document Version
Peer reviewed version

Flex-LCC: A New Grid-Forming HVDC Rectifier for Collecting Large-Scale Renewable Energy

Qianhao Sun, *Member, IEEE*, Qiang Song, *Senior Member, IEEE*, Jingwei Meng, Bin Cui, *Member, IEEE*, Gen Li, *Senior Member, IEEE*, Fan Cheng, and Kailun Wang

***Abstract*—A new grid-forming (GFM) high-voltage direct current (HVdc) rectifier, named flexible line-commutated converter (Flex-LCC), is proposed in this article to collect the power generated by large-scale islanded or weak-grid-supported renewable energy systems. The Flex-LCC uses a series-connected hybrid valve based on the LCC and full-bridge modular multilevel converter (FBMMC), and adopts a new control. As a result, the Flex-LCC works as a GFM rectifier and retains the same dc voltage and power carrying capacity, dc fault clearing, and power reversal functions as an LCC. Particularly, the Flex-LCC has three salient features: the control of the Flex-LCC is decoupled from the LCC part's firing angle, the internal reactive power allocation is flexible, and the valve-side ac voltage of the FBMMC part has a wide operation range due to the decoupling of dc-port voltage and capacitor voltage. These bring reduced interharmonics, enhanced stability, and a smaller capacity boundary to the FBMMC part for the Flex-LCC. Furthermore, utilizing the reasonable design for the actual capacity and valve-side ac voltage of the FBMMC, the Flex-LCC can effectively balance cost, footprint, and weight, and match the current-carrying capacity between the series-connected LCC and FBMMC. The topology, control, characteristics, and design of the Flex-LCC are analyzed in detail in this article. Simulations and experiments validate the theory.**

***Index Terms*—Compact High-voltage direct current (HVdc), flexible line-commutated converter (Flex-LCC), grid-forming control, HVdc hybrid valve, large-scale renewable energy systems (RESs), line-commutated converter (LCC), modular multilevel converter (MMC).**

Manuscript received 29 June 2023; revised 20 September 2023 and 11 October 2023; accepted 14 October 2023. This work was supported in part by the National Key R&D Program of China under Grant 2022YFB2405300 and in part by the National Natural Science Foundation of China under Grant 52307210. *(Corresponding author: Qiang Song.)*

Qianhao Sun, Qiang Song, Jingwei Meng, Bin Cui, and Kailun Wang are with the Department of Electrical Engineering, Tsinghua University, Beijing 100084, China (e-mail: sxsunxianhao@tsinghua.edu.cn; songqiang@tsinghua.edu.cn; mengjw19@mails.tsinghua.edu.cn; cuibin@tsinghua.edu.cn; wkl20@mails.tsinghua.edu.cn).

Gen Li is with the Electric Energy Group, Department of Engineering Technology, Technical University of Denmark (DTU), 2750 Ballerup, Denmark (e-mail: genli@dtu.dk).

Fan Cheng is with the Center for Strategic Studies, Chinese Academy of Engineering, Beijing 100084, China (e-mail: chengfan5566@cae.cn).

Color versions of one or more figures in this article are available at https://doi.org/10.1109/TIE.2023.3327527.

Digital Object Identifier 10.1109/TIE.2023.3327527

I. Introduction

HIGH-VOLTAGE direct current (HVdc) is a feasible solution for collecting and transmitting power generated by long-distance-large-scale renewable energy systems (RESs). The line-commutated converter (LCC) and the voltage source converter (VSC) -based HVdcs are widely used in the current market [1], [2].

The LCC has many merits, such as its large power carrying capacity, high dc voltage withstand capability, lower costs, dc fault clearing ability, etc. However, the LCC has well-known drawbacks: it cannot connect to passive or weak grids and requires a large station footprint [3]. These restrict the application of the LCC-HVdc in integrating islanded or weak-grid-supported RESs. In such cases, VSC-HVdc systems, particularly modular multilevel converter (MMC)-HVdc, are considered more preferable.

However, with the large-demand and high-speed exploitation of RESs, the scale of islanded or weak-grid-supported RESs will continue to increase [4], bringing several severe challenges to MMC-HVdc. First, massive dc capacitors and switches in the MMC results in a high cost and weight [5], [6]. Meanwhile, the compact station footprint advantage of the MMC also gradually diminishes as the capacity increases [7]. Second, too many submodules (SMs) burden the computing of the control system and may even make the MMC unstable. Finally, cables are preferred in half-bridge (HB) MMCs, because the dc fault clearing is not achieved. This leads to very high cost when using the HBMMC in onshore. If overhead lines are chosen, dc circuit breakers or improved MMCs such as full-bridge MMCs (FBMMCs) or hybrid MMCs should be used to protect against dc faults, also significantly increasing the cost [8].

Hybrid valves in [9], [10], [11], [12], [13], and [14] can also be used to integrate large-scale islanded or weak-grid-supported RESs. However, in [9], the high dc voltage also exists in the HBMMC part because of the parallel connection at the dc side. This not only needs numerous SMs but also limits the capacity of the hybrid valve. Then, from another perspective, the series-connected hybrid (SCH) valves are also effective to integrate islanded or weak-grid-supported RESs [10]. The SCH valves were initially used as a receiving end based on a two-level VSC [11]. In [12] and [13], the HBMMC is used to increase the dc voltage and power carrying of the SCH valve further. Recently, a sending-end station based on the SCH valve has been analyzed in [14] to integrate multiple islanded onshore RESs, drawing

on China's Baihetan project [15]. However, in [9], [10], [12], [13], and [14] and in the Baihetan project, the LCC part use its firing angle to achieve the power control, resulting in several challenges for the SCH valve when used to integrate large-scale islanded or weak-grid-supported RESs.

First, dc-link harmonics of the HBMMC will superimpose fluctuations on the control link of the LCC part. This gives rise to the instability and interharmonics for the conventional SCH valve [16]. (In this article, the SCH valve uses the firing angle as a control variable, and the HBMMC as an ancillary circuit is called the conventional SCH valve.) Second, a large firing angle, usually 15°–20°, is required in the conventional SCH valve to regulate the dc voltage or current to always be fixed at a constant value during different conditions, bringing a large reactive power demand of the LCC part, usually 50%–60% of the LCC's active power demand. This will increase the capacity boundary, cost, footprint, and weight of the HBMMC part. Meanwhile, a large capacity of the HBMMC poses a challenge to the current-carrying capacity of full-controlled switches. As a result, multiple HBMMCs may need to be used in parallel, requiring a complex coordination [14]. Finally, the modulation requirement and the current-carrying capacity restriction in full-controlled switches impose a narrow design range on the valve-side ac voltage amplitude of the HBMMC. Otherwise, a large capacity boundary of the HBMMC is required, leading to an increase in cost, footprint, and weight. Or, the capacity demand of the HBMMC will not be satisfied. Usually, the typical dc voltage ratio of the LCC and HBMMC in the conventional SCH valve is 1:1 [12], [13], [14]. However, at present, 1:1 is still too high from matching the current-carrying capacity between the series-connected LCC and HBMMC because the HBMMC still need to transmit half the active power of the whole SCH valve [17].

Considering the current demand for HVdcs integrated with large-scale islanded or weak-grid-supported RESs and the state of technology for the SCH valve, the topology optimization, novel control, and parameter design are proposed in this article for the SCH valve to shape a techno-economic grid-forming (GFM) rectifier. It is worth mentioning that the proposed SCH valve is called flexible LCC (Flex-LCC) in the rest of this article to facilitate the elaboration.

II. Topology and Control Scheme of the Flex-LCC

A. Topology Analysis of the Flex-LCC

The proposed Flex-LCC, a special SCH valve, is presented in Fig. 1(a), where $U_{\rm dc}$, $U_{\rm dcL}$, and $U_{\rm dcM}$ are dc voltages of the Flex-LCC, the LCC part, and the FBMMC part, respectively, $I_{\rm dc}$, $v_{\rm ga,b,c}$, and $i_{\rm ga,b,c}$ are dc-port current, ac-port voltage, and current of the Flex-LCC, $i_{\rm Ma,b,c}$ are valve-side currents of the FBMMC, and $i_{\rm a,b,cp} \sim i_{\rm a,b,cn}$ and $u_{\rm a,b,cp} \sim u_{\rm a,b,cn}$ are arm currents and voltages of the FBMMC. The subscripts "p" and "n" refer to the upper and lower arms, respectively. The LCC part and the FBMMC part in Fig. 1(a) each incorporate converter transformers that have been designed in a manner similar to the transformers used in the conventional LCC and conventional MMC systems, respectively.

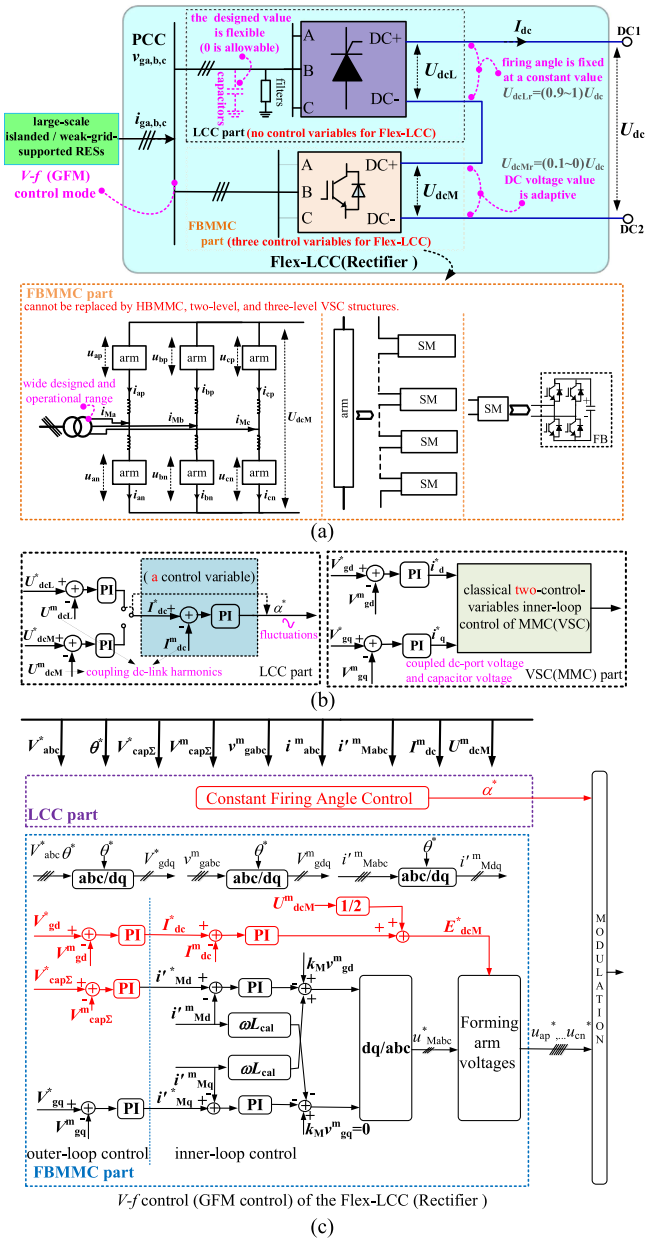

Fig. 1. Topology and control of the Flex-LCC. (a) Topology of the flex-LCC. (b) Control of the conventional SCH valve. (c) Control of the Flex-LCC.

Although the Flex-LCC still uses the SCH valve scheme-based LCC and MMC, the distinguishing topology features of the Flex-LCC lie in the detailed parameter and the irreplaceability of the FBMMC part. That is, the FBMMC part in the Flex-LCC cannot be replaced by the HBMMC or two-level VSC, etc., which is different from the conventional SCH valve. The reason is as follows.

First, the conventional SCH valve uses the firing angle of the LCC to achieve internal power distribution control, and the MMC part uses the common two-control-variables inner loop control [18], [19] to achieve the *V-f* GFM control of the whole SCH valve, as shown in Fig. 1(b). Therefore, the MMC in the conventional SCH valve is a conventional VSC, consequently

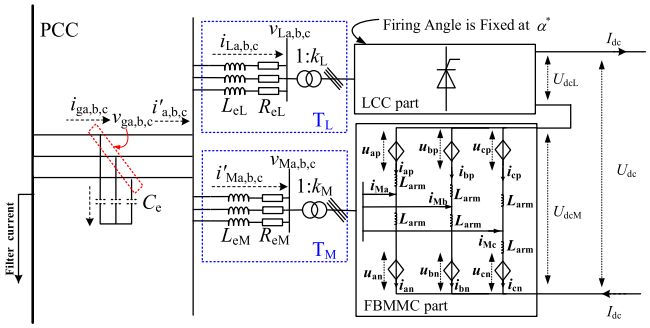

Fig. 2. Analysis model of the proposed Flex-LCC.

allowing it to be replaced by other VSCs. However, in the Flex-LCC, the FBMMC is not only used as a balancer for the internal power distribution but also as a controller for balancing external ac and dc power. Thus, the FBMMC needs to provide three inner-loop control variables for the Flex-LCC when the control of the Flex-LCC is decoupled from the firing angle, as shown in Fig. 1(c). Second, the rated dc voltage and active power for the FBMMC are designed as very low in the Flex-LCC, both within 10% of the Flex-LCC, to reduce costs, footprint, and weight, and facilitates the current-carrying capacity matching for the LCC and FBMMC, which will make the HBMMC unable to work normally due to the modulation restriction, and the coupled control of dc-port voltage and capacitor voltage in Fig. 1(b).

B. Control Scheme of the Flex-LCC

Fig. 1(c) presents the control scheme to achieve Flex-LCC. In Fig. 1(c), "$*$" and "m" refers to the reference and measure value, respectively; "d" and "q" refer to the values of d,q sequence; $V_{\mathrm{cap}\Sigma}$ is the average value of the sum of arm capacitor voltages; V^*_{abc} and θ^* are the amplitude and phase angle of the reference of $v_{\mathrm{ga,b,c}}$; and $i'_{\mathrm{Ma,b,c}}$ is the grid-side current of the FBMMC. The detailed principle about the proposed control is as follows.

The analysis model of the Flex-LCC is presented in Fig. 2, where the converter transformers required for the LCC and FBMMC parts are both modeled as a combination of an ideal transformer with equivalent impedance, labeled as T_{L} and T_{M}, respectively. In Fig. 2, L_{eL} and R_{eL} denote the equivalent inductance and resistance of T_{L}, respectively, while L_{eM} and R_{eM} represent the equivalent inductance and resistance of T_{M}, respectively.

The ac dynamics of the FBMMC in a synchronous frame oriented on $\underline{V}\mathbf{g}$, i.e., $V_{\mathrm{gd}} = V_{\mathrm{g}}$ and $V_{\mathrm{gq}} = 0$ (where $\underline{V}\mathbf{g}$ and V_{g} are the vector and amplitude of $v_{\mathrm{ga,b,c}}$, and $v_{\mathrm{ga,b,c}}$ is the point of common coupling ac three-phase voltage of Flex-LCC), are as follows:

$$\boldsymbol{u}_{\mathbf{Md,q}} = -\left(\frac{L_{\mathrm{arm}}}{2}\frac{d\boldsymbol{i}_{\mathbf{Md,q}}}{dt} + \frac{R_{\mathrm{arm}}}{2}\boldsymbol{i}_{\mathbf{Md,q}}\right) + \omega_{\mathrm{g}}\frac{L_{\mathrm{arm}}}{2}\boldsymbol{J_1}\boldsymbol{i}_{\mathbf{Md,q}} + k_{\mathrm{M}}\boldsymbol{V}_{\mathbf{Md,q}} \tag{1}$$

where $\boldsymbol{x}_{\mathbf{d,q}} = [x_{\mathrm{d}}, x_{\mathrm{q}}]^{\mathrm{T}}$; ω_{g} is the angular frequency of $v_{\mathrm{ga,b,c}}$; i_{Md} and i_{Mq} are the d,q components of $i_{\mathrm{Ma,b,c}}$; $u_{\mathrm{Ma,b,c}}$ is the valve-side voltage of the FBMMC, u_{Md} and u_{Mq} are the d,q components of $u_{\mathrm{Ma,b,c}}$; L_{arm} and R_{arm} are the arm inductance and resistance of the FBMMC; k_{M} is the transformer turns ratio of the FBMMC; $v_{\mathrm{Ma,b,c}}$ is the grid-side voltage of the FBMMC, V_{Md}, V_{Mq} are the d,q components of $v_{\mathrm{Ma,b,c}}$; and $\boldsymbol{J_1}$ is the coefficient.

Meanwhile, $u_{\mathrm{Ma,b,c}}$ and $\boldsymbol{J_1}$ are

$$u_{\mathrm{Ma,b,c}} = \frac{u_{\mathrm{a,b,cn}} - u_{\mathrm{a,b,cp}}}{2} \quad \boldsymbol{J_1} = \begin{bmatrix} 0 & 1 \\ -1 & 0 \end{bmatrix} \tag{2}$$

where $u_{\mathrm{a,b,cn}}$ and $u_{\mathrm{a,b,cp}}$ are the arm voltages of the FBMMC part.

Then, considering the relationship of $i'_{\mathrm{Ma,b,c}}$ and $i_{\mathrm{Ma,b,c}}$

$$i_{\mathrm{Mabc}} = \frac{i'_{\mathrm{Mbac}}}{k_{\mathrm{M}}} \Rightarrow \left\{ i_{\mathrm{Md}} = \frac{i'_{\mathrm{Md}}}{k_{\mathrm{M}}} \quad i_{\mathrm{Mq}} = \frac{i'_{\mathrm{Mq}}}{k_{\mathrm{M}}} \right\} \tag{3}$$

where i'_{Md} and i'_{Mq} are the d,q components of $i'_{\mathrm{Ma,b,c}}$.

Equation (1) can be transformed to

$$\boldsymbol{u}_{\mathbf{Md,q}} = -\left(\frac{L_{\mathrm{arm}}}{2k_{\mathrm{M}}}\frac{d\boldsymbol{i}'_{\mathbf{Md,q}}}{dt} + \frac{R_{\mathrm{arm}}}{2k_{\mathrm{M}}}\boldsymbol{i}'_{\mathbf{Md,q}}\right) + \omega_{\mathrm{g}}\frac{L_{\mathrm{arm}}}{2k_{\mathrm{M}}}\boldsymbol{J_1}\boldsymbol{i}'_{\mathbf{Md,q}} + k_{\mathrm{M}}\boldsymbol{V}_{\mathbf{Md,q}}. \tag{4}$$

Because $v_{\mathrm{ga,b,c}}$ and $v_{\mathrm{Ma,b,c}}$ have the following relationship:

$$\boldsymbol{V}_{\mathbf{Md,q}} = -\left(L_{\mathrm{eM}}\frac{d\boldsymbol{i}'_{\mathbf{Md,q}}}{dt} + R_{\mathrm{eM}}\boldsymbol{i}'_{\mathbf{Md,q}}\right) + \omega_{\mathrm{g}}L_{\mathrm{eM}}\boldsymbol{J_1}\boldsymbol{i}'_{\mathbf{Md,q}} + \boldsymbol{V}_{\mathbf{gd,q}} \tag{5}$$

(4) can be further transformed to

$$\boldsymbol{u}_{\mathbf{Md,q}} = -\left(L_{\mathrm{cal}}\frac{d\boldsymbol{i}'_{\mathbf{Md,q}}}{dt} + R_{\mathrm{cal}}\boldsymbol{i}'_{\mathbf{Md,q}}\right) + \omega_{\mathrm{g}}L_{\mathrm{cal}}\boldsymbol{J_1}\boldsymbol{i}'_{\mathbf{Md,q}} + k_{\mathrm{M}}\boldsymbol{V}_{\mathbf{gd,q}} \tag{6}$$

where L_{cal} and R_{cal} represent the equivalent inductance and resistance of the Flex-LCC, and can be calculated as

$$L_{\mathrm{cal}} = k_{\mathrm{M}}L_{\mathrm{eM}} + \frac{L_{\mathrm{arm}}}{2k_{\mathrm{M}}} \quad R_{\mathrm{cal}} = k_{\mathrm{M}}R_{\mathrm{eM}} + \frac{R_{\mathrm{arm}}}{2k_{\mathrm{M}}}. \tag{7}$$

Because the regulating variates of the FBMMC part are $u_{\mathrm{a,b,cn}}$ and $u_{\mathrm{a,b,cp}}$, to decouple them, a voltage E_{dcM} is defined as

$$E_{\mathrm{dcM}} = \frac{u_{\mathrm{a,b,cn}} + u_{\mathrm{a,b,cp}}}{2}. \tag{8}$$

Then, arm voltages $u_{\mathrm{a,b,cn}}$ and $u_{\mathrm{a,b,cp}}$ can be derived as

$$u_{\mathrm{a,b,cn}} = E_{\mathrm{dcM}} + u_{\mathrm{Ma,b,c}} \quad u_{\mathrm{a,b,cp}} = E_{\mathrm{dcM}} - u_{\mathrm{Ma,b,c}}. \tag{9}$$

In addition, the dc dynamics of the FBMMC part are

$$E_{\mathrm{dcM}} = \frac{L_{\mathrm{arm}}}{6}\frac{dI_{\mathrm{dc}}}{dt} - \frac{L_{\mathrm{arm}}}{2}\frac{di_{\mathrm{cirabc}}}{dt} + \frac{U_{\mathrm{dcM}}}{2} \tag{10}$$

where $i_{\mathrm{cira,b,c}}$ are arm circulating currents of the FBMMC part.

Ignoring circulating currents, (10) can be transformed to

$$E_{\mathrm{dcM}} = \frac{L_{\mathrm{arm}}}{6}\frac{dI_{\mathrm{dc}}}{dt} + \frac{U_{\mathrm{dcM}}}{2}. \tag{11}$$

At last, considering the LCC part in the Flex-LCC

$$\text{ac}: \begin{cases} \boldsymbol{V}_{\mathbf{Ld,q}} = -(L_{\text{eL}}\frac{d\boldsymbol{i}_{\mathbf{Ld,q}}}{dt} + R_{\text{eL}}\boldsymbol{i}_{\mathbf{Ld,q}}) + \omega_{\text{g}}L_{\text{eL}}\boldsymbol{J}_1\boldsymbol{i}_{\mathbf{Ld,q}} \\ \quad +\boldsymbol{V}_{\mathbf{gd,q}} \\ \boldsymbol{i}_{\mathbf{gd,q}} = C_{\text{e}}\boldsymbol{J}_2\frac{d\boldsymbol{V}_{\mathbf{gd,q}}}{dt} + \omega_{\text{g}}C_{\text{e}}\boldsymbol{J}_3\boldsymbol{V}_{\mathbf{gd,q}} + \boldsymbol{i}_{\mathbf{Ld,q}} + \boldsymbol{i}'_{\mathbf{Md,q}} \end{cases} \tag{12}$$

where C_{e} is the equivalent capacitor of ac reactive power compensation capacitor and filter banks, $\boldsymbol{J_2}$ and $\boldsymbol{J_3}$ both are the coefficient matrixes, and can be derived as

$$\boldsymbol{J}_2 = \begin{bmatrix} 1 & 0 \\ 0 & 1 \end{bmatrix} \quad \boldsymbol{J}_3 = \begin{bmatrix} 0 & 1 \\ 1 & 0 \end{bmatrix} \tag{13}$$

and

$$\text{dc}: \begin{cases} U_{\text{dcL}} = \frac{6\sqrt{3}k_{\text{L}}\sqrt{V_{\text{gd}}^2+V_{\text{gq}}^2}\cos\alpha^*}{\pi} - \frac{6k_{\text{L}}^2\omega_{\text{g}}L_{\text{eL}}I_{\text{dc}}}{\pi} \\ U_{\text{dcM}} = U_{\text{dc}} - U_{\text{dcL}} \end{cases} \tag{14}$$

where $\alpha*$ and k_{L} are the firing angle and transformer turns ratio of the LCC part.

Based on (6), (11)–(14), the overall control scheme of the Flex-LCC can be designed as Fig. 1(c). Obviously, in Fig. 1(c), the FBMMC not only provides two control variables to balance the active and reactive power between ac and dc terminals of the Flex-LCC, but also provides one control variable for achieving the power distribution between the internal LCC and FBMMC. Thus, the firing angle of the LCC part in Flex-LCC can be fixed at a constant value, as shown in Fig. 1(c), which is impossible for the conventional SCH valve, which uses the control in Fig. 1(b). Meanwhile, Fig. 1(c) shows the dc-port voltage and capacitor voltage of the FBMMC part in the Flex-LCC is decoupled due to the fact that the capacitor voltage is controlled actively to follow its reference value when the dc-port voltage of the FBMMC part is changed adaptively ($U_{\text{dcM}} = U_{\text{dc}}$-$U_{\text{dcL}}$). Then, based on this characteristic, the valve-side ac voltage of the FBMMC ($k_{\text{M}}V_{\text{g}}$) can operate over a wide range and is not limited to $0.5U_{\text{dcM}}$, which is usually designed in the conventional SCH valve.

In the conventional SCH valve, the rated value of α usually is designed as 15°∼20° to ensure stable control, bringing a large reactive power boundary of the LCC, usually 50%∼60% of the LCC's active power demand. As stated in [9], this high reactive power boundary poses challenges for the conventional SCH valve because the current current-carrying capacity of the MMC cannot match that of the LCC. However, Fig. 1(c) demonstrates that the firing angle of the LCC part in the Flex-LCC can operate at any value in theory. Therefore, by utilizing the designed value of $\alpha*$ in the Flex-LCC, it is possible to reduce the internal capacity boundary of the FBMMC, facilitating the current-carrying capacity between the series-connected LCC and FBMMC and optimizing the cost, footprint, and weight of the Flex-LCC. The detailed analysis is shown as Section III. In addition, when comparing Fig. 1(b) and (c), it is obvious that the firing angle in the conventional SCH valve experiences fluctuations due to closed-loop control of α. This coupling of dc-link harmonics into the control link introduces interharmonics, losses, and instability to the whole SCH valve. These adverse fluctuations will not occur in the Flex-LCC because the firing angle is not used as a closed-loop control variable to regulate the power, there is no operation and control link to couple the dc-link harmonics to the control link of the LCC part.

III. Characteristics and Design of the Flex-LCC

A. Internal Power Demand Boundaries Analysis

In the Flex-LCC, the equivalent relationships between V_{g} and V_{gd}, V_{gq} are as follows:

$$V_{\text{g}} = \sqrt{V_{\text{gd}}^2 + V_{\text{gq}}^2}. \tag{15}$$

Thus, (14) can be transformed to

$$\begin{cases} U_{\text{dcL}} = \frac{6\sqrt{3}}{\pi}k_{\text{L}}V_{\text{g}}\cos\alpha^* - \frac{6}{\pi}k_{\text{L}}^2\omega_{\text{g}}L_{\text{eL}}\frac{P_{\text{Flex-LCC}}}{U_{\text{dc}}} \\ U_{\text{dcM}} = U_{\text{dc}} - \frac{6\sqrt{3}}{\pi}k_{\text{L}}V_{\text{g}}\cos\alpha^* + \frac{6}{\pi}k_{\text{L}}^2\omega_{\text{g}}L_{\text{eL}}\frac{P_{\text{Flex-LCC}}}{U_{\text{dc}}} \end{cases} \tag{16}$$

where $P_{\text{Flex-LCC}}$ is the active power value of the Flex-LCC.

Based on (16), U_{dcL} reaches its minimum boundary (U_{dcLr}) and U_{dcM} reaches its maximum boundary (U_{dcMr}) when the power of the Flex-LCC is at its maximum ($P_{\text{rFlex-LCC}}$). Conversely, U_{dcL} reaches its maximum boundary (U_{dcL0}) and U_{dcM} reaches its maximum boundary (U_{dcM0}) when the power of the Flex-LCC is at 0. That is to say

$$\begin{cases} U_{\text{dcLr}} = \frac{6\sqrt{3}}{\pi}k_{\text{L}}V_{\text{g}}\cos\alpha^* - \frac{6}{\pi}k_{\text{L}}^2\omega_{\text{g}}L_{\text{eL}}\frac{P_{\text{rFlex-LCC}}}{U_{\text{dc}}} \\ U_{\text{dcMr}} = U_{\text{dc}} - U_{\text{dcLr}} \end{cases} \tag{17-1}$$

and

$$\begin{cases} U_{\text{dcL0}} = \frac{6\sqrt{3}}{\pi}k_{\text{L}}V_{\text{g}}\cos\alpha^* \\ U_{\text{dcM0}} = U_{\text{dc}} - U_{\text{dcL0}} \end{cases}. \tag{17-2}$$

According to (17), the internal active power demand boundaries $P_{\text{LCC\_max}}$ and $P_{\text{MMC\_max}}$ in the Flex-LCC are

$$\begin{cases} P_{\text{LCC\_max}} = \frac{6\sqrt{3}k_{\text{L}}V_{\text{g}}\cos\alpha^*P_{r\text{Flex-LCC}}}{\pi U_{\text{dc}}} - \frac{6k_{\text{L}}^2\omega_{\text{g}}L_{\text{eL}}P_{\text{rFlex-LCC}}^2}{\pi U_{\text{dc}}^2} \\ P_{\text{MMC\_max}} = P_{r\text{Flex-LCC}} - P_{\text{LCC\_max}} \end{cases}. \tag{18}$$

The internal reactive power demand boundaries $Q_{\text{MMC\_max}}$ and $Q_{\text{LCC\_max}}$ are

$$Q_{\text{MMC\_max}} = Q_{\text{LCC\_max}} = P_{\text{LCC\_max}}\tan\phi \tag{19}$$

where ϕ is the power factor angle of the LCC part, and is

$$\begin{cases} \cos\phi = \frac{1}{2}\left[\cos(\alpha^*) + \cos(\alpha^*+\mu)\right] \\ \mu = \arccos(\cos(\alpha^*) - \frac{2\omega_{\text{g}}L_{\text{eL}}P_{\text{rFlex-LCC}}}{\sqrt{3}k_{\text{L}}V_{\text{g}}U_{\text{dc}}}) - \alpha^* \end{cases} \tag{20}$$

where μ is the overlapping angle of commutation.

Equations (18)–(20) can be standardized as

$$\begin{cases} P_{\text{LCC\_max}}^{\text{p.u.}} = k_{\text{L}}^{\text{p.u.}} - \frac{\pi(\omega_{\text{g}}L_{\text{eL}})^{\text{p.u.}}\left(k_{\text{L}}^{\text{p.u.}}\right)^2}{18}\frac{1}{\cos^2\alpha^*} \\ P_{\text{MMC\_max}}^{\text{p.u.}} = 1 - P_{\text{LCC\_max}}^{\text{p.u.}} \\ Q_{\text{MMC\_max}}^{\text{p.u.}} = Q_{\text{LCC\_max}}^{\text{p.u.}} = P_{\text{LCC\_max}}^{\text{p.u.}}\tan\phi \\ \cos\phi = \cos(\alpha^*) - \frac{6\cos\alpha^*(\omega_{\text{g}}L_{\text{eL}})^{\text{p.u.}}}{\pi k_{\text{L}}^{\text{p.u.}}}\left(\frac{V_{\text{g}}}{U_{\text{dc}}}\right)^2 \end{cases} \tag{21}$$

where

$$\begin{cases} P_{\text{LCC\_max}}^{\text{p.u.}} = \frac{P_{\text{LCC\_max}}}{P_{r\text{Flex-LCC}}} \quad P_{\text{MMC\_max}}^{\text{p.u.}} = \frac{P_{\text{MMC\_max}}}{P_{r\text{Flex-LCC}}} \\ Q_{\text{MMC\_max}}^{\text{p.u.}} = Q_{\text{LCC\_max}}^{\text{p.u.}} = \frac{Q_{\text{LCC\_max}}}{P_{r\text{Flex-LCC}}} \\ k_{\text{L}}^{\text{p.u.}} = \frac{U_{\text{dcL0}}}{U_{\text{dc}}} \quad (\omega_{\text{g}}L_{\text{eL}})^{\text{p.u.}} = \frac{\omega_{\text{g}}L_{\text{eL}}P_{\text{rFlex-LCC}}}{V_{\text{g}}^2} \end{cases}. \tag{22}$$

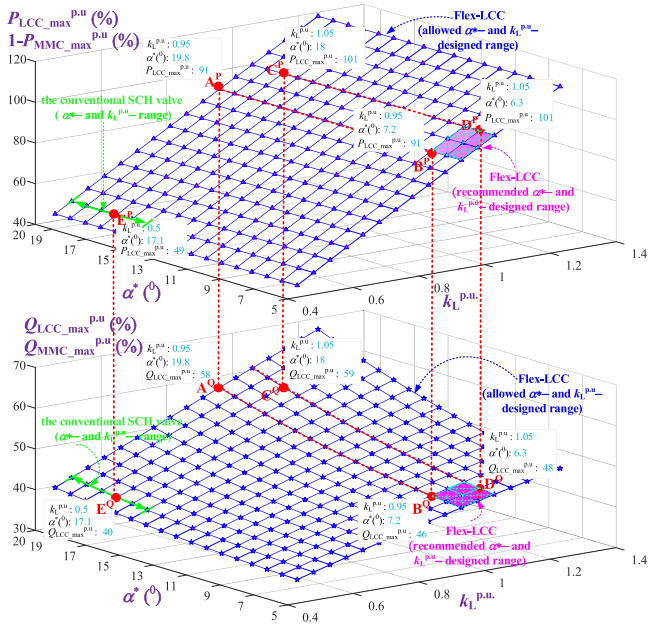

Fig. 3. α^*- and $k_{\mathrm{L}}{}^{\mathrm{p.u.}}-$ design analysis for the Flex-LCC.

Then, the corresponding curves are presented as Fig. 3, where the internal active power boundaries of the LCC and FBMMC in Flex-LCC both remain almost unchanged with the change of α^* when $k_{\mathrm{L}}{}^{\mathrm{p.u.}}$ is a certain value, such as $\mathrm{A^P}$ and $\mathrm{B^P}$, $\mathrm{C^P}$ and $\mathrm{D^P}$. Meanwhile, $P_{\mathrm{LCC\_max}}{}^{\mathrm{p.u}}$ (1-$P_{\mathrm{MMC\_max}}{}^{\mathrm{p.u}}$) in the Flex-LCC is always smaller than $k_{\mathrm{L}}{}^{\mathrm{p.u}}$, such as $\mathrm{E^P}$, which is in contrast to the conventional SCH valve where $P_{\mathrm{LCC\_max}}{}^{\mathrm{p.u}} = k_{\mathrm{L}}{}^{\mathrm{p.u}}$. Meanwhile, the internal reactive power boundaries of the LCC and FBMMC in the Flex-LCC both increase with the increasing of α^* when $k_{\mathrm{L}}{}^{\mathrm{p.u.}}$ is a certain value, such as $\mathrm{A^Q}$ and $\mathrm{B^Q}$, $\mathrm{C^Q}$ and $\mathrm{D^Q}$. Thus, to minimize the capacity (mainly the reactive power capacity) boundary of the FBMMC in the Flex-LCC as much as possible, α^* should be as small as possible. Considering the practical limitation, α^* in the Flex-LCC is recommended to 5°∼7° to satisfy the turn-OFF time of thyristors.

In addition, for the conventional SCH valve, $k_{\mathrm{L}}{}^{\mathrm{p.u.}}$ usually is designed as 0.5 when the rated α^* is usually designed as 15°∼20°, as shown by the green lines in Fig. 3. However, for the Flex-LCC, not only is α^* able to be extended to the minimum value, but also the design range of $k_{\mathrm{L}}{}^{\mathrm{p.u.}}$ can be extended, as shown by blue lines in Fig. 3. Thus, $k_{\mathrm{L}}{}^{\mathrm{p.u.}}$ can also be used to further reduce the capacity boundary (mainly the active power boundary) of the FBMMC in the Flex-LCC when α^* is selected.

For the FBMMC part in the Flex-LCC, because

$$S_{\mathrm{MMC\_max}}^{\mathrm{p.u.}} = \sqrt{\left(P_{\mathrm{MMC\_max}}^{\mathrm{p.u.}}\right)^2 + \left(Q_{\mathrm{MMC\_max}}^{\mathrm{p.u.}}\right)^2}. \tag{23}$$

Then, according to (21)–(23), the value of $k_{\mathrm{L}}{}^{\mathrm{p.u.}}$ that minimizes the capacity of the FBMMC can be calculated when α^* is selected. In practical applications, the exact $k_{\mathrm{L}}{}^{\mathrm{p.u.}}$ in (23) can be replaced by a range of $k_{\mathrm{L}}{}^{\mathrm{p.u}}$, which makes $P_{\mathrm{LCC\_max}}{}^{\mathrm{p.u}}$ (1-$P_{\mathrm{MMC\_max}}{}^{\mathrm{p.u}}$), i.e., $U_{\mathrm{dcLr}}/U_{\mathrm{dc}}$ ((17)) is in 0.9 ∼ 1 to simplify the design.

According to the aforementioned analysis, α^* and $k_{\mathrm{L}}{}^{\mathrm{p.u.}}$ in the Flex-LCC both can be used to reduce the capacity demand boundary of the FBMMC part, i.e., α^* is used mainly to reduce the reactive power demand and $k_{\mathrm{L}}{}^{\mathrm{p.u}}$ is used mainly to reduce the active power demand. Then, the capacity boundary of the FBMMC in the Flex-LCC will be obviously smaller than that of the MMC in the conventional SCH valve. Based on Fig. 3, the internal capacity boundary of the MMC part in the Flex-LCC can be reduced from 66% (64%) $\mathrm{P_{rFlex\text{-}LCC}}$ to 46% (45%) $\mathrm{P_{rFlex\text{-}LCC}}$, compared with the conventional SCH valve. That is, approximately 30% of the capacity boundary can be reduced for the MMC part in the Flex-LCC. The reduced internal capacity boundary of the MMC part in the Flex-LCC will reduce the current-carrying capacity demand of full-controlled switches, facilitating the matching of current-carrying capacity between the LCC and FBMMC in the Flex-LCC. Meanwhile, the cost, footprint, and weight of the whole SCH valve will also be reduced with the reduction of the capacity demand of the MMC part.

B. Reactive Power Capacity Configuration Analysis

In the Flex-LCC, to satisfy the internal reactive power demand of the LCC part, the FBMMC and ac capacitor banks both can be used

$$Q_{\mathrm{MMC\_max}} = Q_{\mathrm{LCC\_max}} = \langle Q_{\mathrm{MMC}} \rangle + \langle Q_{\mathrm{bank}} \rangle \tag{24}$$

where $<Q_{\mathrm{MMC}}>$ and $<Q_{\mathrm{bank}}>$ are the designed reactive power capacity for the FBMMC and ac capacitor banks.

Equation (24) shows that two ways can be used to compensate the internal reactive power demand in Flex-LCC: One uses the FBMMC part and the other uses the ac capacitor banks. Therefore, in the Flex-LCC, the allocation of the reactive power capacity for the FBMMC part and the ac capacitor banks can be adjusted to ensure that the current-carrying capacity of the LCC and FBMMC match each other. This can be achieved by increasing the designed value of the reactive power capacity for the ac capacitor banks. However, based on engineering experiences [20], [21], [22], the allocation of the internal reactive power capacity will obviously have an impact on the cost, footprint, and weight of the Flex-LCC.

To quantitatively represent the deigned allocation of the internal reactive power capacity in the Flex-LCC, q_{M}, the designed reactive power capacity ratio of the FBMMC part is defined as

$$\begin{cases} q_{\mathrm{M}} = \dfrac{\langle Q_{\mathrm{MMC}} \rangle}{Q_{\mathrm{MMC\_max}}} = 1 - \dfrac{\langle Q_{\mathrm{bank}} \rangle}{Q_{\mathrm{MMC\_max}}} \\ \langle Q_{\mathrm{bank}} \rangle = \langle N_{\mathrm{C}} \rangle \langle n_{\mathrm{C}} \rangle \langle Q_{\mathrm{bank\_unit}} \rangle \end{cases} \tag{25}$$

where ac capacitor banks are divided into $<N_{\mathrm{C}}>$ larger groups, and each larger group has $<n_{\mathrm{C}}>$ smaller groups. $<Q_{\mathrm{bank\_unit}}>$ is the minimum switching reactive power unit of ac capacitor banks.

To achieve the *V-f* GFM control, the Flex-LCC needs to have a continuous reactive power output, i.e., q_{M} needs to satisfy

$$\frac{\langle Q_{\mathrm{bank\_unit}} \rangle}{Q_{\mathrm{MMC\_max}}} \le q_{\mathrm{M}} \le 1. \tag{26}$$

In the Flex-LCC, using ac capacitor banks to compensate for internal reactive power is a cost-effective option. However, it comes with the drawback of a large footprint, and the reactive power regulation is discontinuous. On the contrary, using the FBMMC part offers continuous reactive power regulation and a compact footprint, albeit at a higher cost. Then, given that the cost of land or offshore platforms has a positive correlation with the footprint, the value of q_{M} should be comprehensively chosen by considering the cost, footprint, and the limitation for the current-carrying capacity matching of the series-connected LCC and FBMMC in the Flex-LCC.

C. Valve-Side AC Voltage Amplitude Selection for the FBMMC

For the FBMMC in the Flex-LCC, the root mean square (rms) value and maximum value of arm currents are

$$\begin{cases} \mathrm{RMS}_{i_{\mathrm{a,b,cp,n}}} = \frac{1}{3}\sqrt{\left(\frac{P_{r\mathrm{Flex-LCC}}}{U_{\mathrm{dc}}}\right)^2 + \frac{1}{2}\left(\frac{\langle S_{\mathrm{MMC}}\rangle}{k_{\mathrm{M}}V_{\mathrm{g}}}\right)^2} \\ \mathrm{MAX}_{i_{\mathrm{a,b,cp,n}}} = \frac{1}{3}\left(\frac{P_{r\mathrm{Flex-LCC}}}{U_{\mathrm{dc}}} + \frac{\langle S_{\mathrm{MMC}}\rangle}{k_{\mathrm{M}}V_{\mathrm{g}}}\right) \end{cases} \tag{27}$$

where $<S_{\mathrm{MMC}}>$ is the actual design capacity of the FBMMC in the Flex-LCC, and can be derived as

$$\langle S_{\mathrm{MMC}}\rangle = \sqrt{(P_{\mathrm{MMC\_max}})^2 + (q_{\mathrm{M}}Q_{\mathrm{MMC\_max}})^2}. \tag{28}$$

Based on (27) and (28), the valve-side ac voltage of the FBMMC part can be used to further reduce the current-carrying capacity demand of full-controlled switches when the actual capacity of the FBMMC part is determined (i.e., $P_{\mathrm{MMC\cdot max}}$, $Q_{\mathrm{MMC\cdot max}}$, and q_{M} are determined)

$$k_{\mathrm{M}} \geq \max\left[\frac{\frac{\langle S_{\mathrm{MMC}}\rangle U_{\mathrm{dc}}}{P_{r\mathrm{Flex-LCC}}V_{\mathrm{g}}}}{\sqrt{2\left(\left(\frac{3\mathrm{RMS}_{\mathrm{sch}}U_{\mathrm{dc}}}{P_{r\mathrm{Flex-LCC}}}\right)^2 - 1\right)}}, \frac{\frac{\langle S_{\mathrm{MMC}}\rangle U_{\mathrm{dc}}}{P_{r\mathrm{Flex-LCC}}V_{\mathrm{g}}}}{\frac{3U_{\mathrm{dc}}\mathrm{MAX}_{\mathrm{sch}}}{P_{r\mathrm{Flex-LCC}}} - 1}\right] \tag{29}$$

where $\mathrm{RMS}_{\mathrm{sch}}$ and $\mathrm{MAX}_{\mathrm{sch}}$ are the limitations of rms value and maximum value for the full-controlled switches used in the FBMMC; the output of **max** $[x,y]$ is the larger value of x and y.

Then, the reference value of the sum of arm capacitor voltages in the FBMMC part can be designed as

$$V^*_{\mathrm{cap}\Sigma} \geq 0.5U_{\mathrm{dc}}\max\left[P^{\mathrm{p.u.}}_{\mathrm{MMC\_max}}, |1 - k^{\mathrm{p.u.}}_{\mathrm{L}}|\right] + k_{\mathrm{M}}V_{\mathrm{g}}. \tag{30}$$

Based on (30), the SM number per arm and capacitance per SM, etc., parameters for the FBMMC in the Flex-LCC can be calculated.

D. Parameter Design Analysis for the Flex-LCC

According to Section III.A–C, the discussed three salient characteristics of the Flex-LCC, the reduced internal capacity boundary for the FBMMC, the flexible reactive power allocation ratio, and the wide operation range of the valve-side ac voltage amplitude for the FBMMC, all facilitate the matching of the current-carrying capacity between the LCC and FBMMC and the optimization of the cost, footprint, and weight of the Flex-LCC. Then, the detailed design method that utilizes these three features to optimize the performance of the Flex-LCC is shown in Fig. 4.

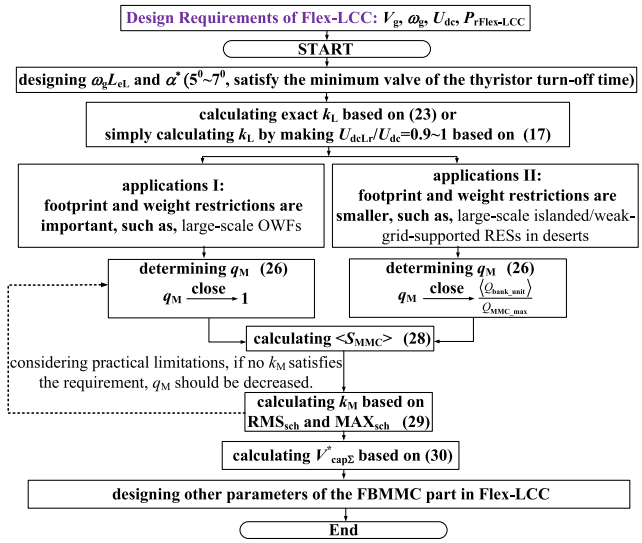

Fig. 4. Key parameters design of the Flex-LCC.

IV. Case Study of the Flex-LCC

A. Case I: The Flex-LCC Used to Integrate Large-Scale Offshore Wind Farms (OWFs)

As OWFs develop further into deep waters, the capacity will continue to increase, leading to a corresponding increase in the required capacity of offshore HVdc stations. Then, as mentioned in [5], [6], and [7], the cost, footprint, and weight of HBMMC-based stations will be challenged by this trend. In such applications, the Flex-LCC can be used to construct a new type of offshore station for integrating large-scale OWFs.

Assuming a Flex-LCC with 1500 MW, ±400 kV is required to integrate OWFs. According to Fig. 4, the key parameters are designed as shown in Table I, where the valve-side ac voltage (104 kV) of the FBMMC is no longer 0.5 times of its dc voltage (25 kV), which is obviously different from the conventional design of MMCs. In addition, when the capacity is the same, assuming the cost and footprint of the LCC station (without ac capacitor and filter banks) are 60% and 30% of those of the HBMMC [5], [20], [21], [23], The Flex-LCC can reduce the cost by approximately 10% and the footprint by approximately 30% when compared to the HBMMC. Meanwhile, the weight of the Flex-LCC is obviously also smaller than that of the HBMMC station. These are all highly advantageous for the construction of offshore platforms.

B. Case II: Flex-LCC Used to Integrate Onshore (such as Deserts) Large-Scale Islanded or Weak-Grid-Supported RES Bases

In China, the consumption of power from large-scale RES bases has become an important and key demand now. Particularly, the utilization of photovoltaics and wind power in

TABLE I
MAIN PARAMETERS OF THE FLEX-LCC IN CASES I AND II

Parameters	Case I	Case II
$\sqrt{3/2}V_g$, ω_g	66 kV, 50 Hz	66 kV, 50 Hz
U_{dc}, $P_{rFlex\text{-}LCC}$	±400 kV, 1500 MW	800 kV, 4000 MW
α^*	6^0	6^0
$k_L^{p.u.}$	1.03 (U_{dcL0}=825 kV)	1.03 (U_{dcL0}=825 kV)
Rated dc voltages of LCC, FBMMC	780 kV, ±25 kV	785 kV, ±25 kV
q_M	0.84	0.1
Capacity of LCC	1480 MW,500 MVar	3940 MW,1300 MVar
Capacity of FBMMC	50 MW, 420 MVar	80 MW, 130 MVar
SM voltage	2 kV	2 kV
$V^*_{cap\Sigma}$	130 kV	180 kV
Number of SMs	65	90
Equivalent switching frequency	430 Hz	430 Hz
Maximum reactive power of ac filters	80 MVar	240 MVar
Maximum reactive power of ac capacitor banks	/	1020 MVar
Winding structure of T_L	Yg/Y/D1	Yg/Y/D1
Winding structure of T_M	D1/Yg	D1/Yg
Nominal capacity of T_L	1600 MVA	4200 MVA
Nominal capacity of T_M	500 MVA	250 MVA
frequency of T_L, T_M	50 Hz	50 Hz
k_L	66 kV/308 kV	66 kV/308 kV
k_M	66 kV/104 kV	66 kV/160 kV
Leakage inductance of T_L	0.20 (p.u.)	0.17 (p.u.)
Leakage inductance of T_M	0.15 (p.u.)	0.10 (p.u.)
RMS_{sch}, MAX_{sch}	1.8 kA, 3 kA	1.8 kA, 3 kA
Short-circuit ratio of the ac system in simulation verification	islanded system	1.2

Notes: In Table I, $U_{dcL0}= k_L^{p.u.}U_{dc}$ represents the maximum allowable dc voltage for the LCC part in Flex-LCC, while the minimum allowable dc voltage for the LCC part is its rated dc voltage.

deserts has been clearly planned in China's 14th Five-Year Plan (2021–2025). The large-scale RES bases in deserts are typically islanded or weak-grid-supported RESs, challenging the application of LCC-HVdc without sufficient auxiliary thermal power plants. Meanwhile, as mentioned in [2], [7], and [8], MMC-HVdc also faces severe challenges in terms of cost, dc fault clearing, and power carrying capacity, etc., when used to integrate onshore large-scale islanded or weak-grid-supported RES bases. In such applications, the Flex-LCC is a feasible scheme.

Assuming a Flex-LCC with 4000 MW, 800 kV (single-pole converter station in a bipolar UHVdc with 8000 MW, ±800 kV) is required to integrate large-scale RES bases in deserts. Then, the parameters are designed as shown in Table I, where the minimum switching reactive power unit of ac capacitor banks $<Q_{bank\_unit}>$ is designed as $1/(4 \times 4)$ of $<Q_{bank}>$. In Table I, the dc voltage and capacity for the FBMMC both are less than 5% of those in the Flex-LCC. Therefore, the cost of the Flex-LCC is smaller, compared with HBMMC, and the current-carrying capacity matching between the LCC and FBMMC can be achieved easily. Meanwhile, the *V-f* GFM control is also achieved by the Flex-LCC.

V. SIMULATION AND EXPERIMENTAL VERIFICATION

A. Simulation Results

To validate the theory, models based on the parameters provided in Table I were constructed using MATLAB/Simulink, and the detailed results are presented in Fig. 5.

Fig. 5(a) shows the simulation results of the Flex-LCC in Case I. The frequency and amplitude of the ac terminal voltage of the Flex-LCC are actively controlled at 50 Hz and 66 kV, respectively, when the dc terminal voltage (800 kV) and power of Flex-LCC both depend on the external system. Meanwhile, the internal dc voltage and active power of the Flex-LCC are distributed adaptively. Such as, when $P_{\text{Flex-LCC}} = 1500$ MW, $P_{\text{LCC}} = 1470$ MW, $P_{\text{MMC}} = 30$ MW, $U_{\text{dcL}} = 783$ kV, and $U_{\text{dcM}} = 17$ kV; when $P_{\text{Flex-LCC}} = 151$ MW, $P_{\text{LCC}} = 150$ MW, $P_{\text{MMC}} = -2$ MW, $U_{\text{dcL}} = 820$ kV, and $U_{\text{dcM}} = -20$ kV. Obviously, the rated active power and dc voltage ratios of the FBMMC both less than 5% of that of the Flex-LCC. In addition, the aforementioned ratios in the Flex-LCC both are varied with the power, which is obviously different with a conventional SCH valve. For example, when $P_{\text{Flex-LCC}} = 1500$ MW, the active power ratio of the FBMMC is 2%; when $P_{\text{Flex-LCC}} = 151$ MW, that is −1.3%.

Fig. 5(a) also shows that the reactive power demand of the LCC part inside the Flex-LCC-Case I is mainly provided by the FBMMC. Moreover, the LCC's rated reactive power in the Flex-LCC is about 33% (492/1470), which is obviously less than that in a conventional SCH valve (50%∼60%). Meanwhile, the maximum value and rms value of arm currents in the Flex-LCC-Case I is less than 3 and 1.8 kA, respectively, both meet requirements for the current-carrying capacity of full-controlled switches in the current engineer. In addition, Fig. 5(a) shows the firing angle in the Flex-LCC-Case I keeps at 6°, and there is no fluctuation in the firing angle, which is also consistent with the theoretical analysis.

Fig. 5(b) shows the simulation results of the Flex-LCC in case II. In Fig. 5(b), the *V-f* GFM control of the Flex-LCC is also achieved. Meanwhile, the rules of internal dc voltage and active power of the Flex-LCC-Case II are similar to those in Case I, and maximum and rms values of current in the full-controlled switches also meet the current engineering demand. The main difference of Flex-LCC-Case II and -Case I lies on the reactive power of the FBMMC part. In Fig. 5(b), the reactive power of the LCC part is mainly provided by the ac capacitor banks, and the FBMMC only provide 1.3% (15/1245) reactive power when the active power is at the rated value. Therefore, the rated capacity of the FBMMC part in the Flex-LCC-Case II is very low, as shown in Table I, about 3.8% of the whole power. That is, the Flex-LCC-Case II provides a techno-economic scheme to construct an onshore 4000 MW, 800 kV-GFM VSC based on a main-body LCC and an auxiliary 150 MVA-FBMMC. To the best of the author's knowledge, such a large capacity and high dc voltage is very challenging for the existing MMCs due to the current-carrying capacity limitation of full-controlled switches.

Moreover, it should be noted that in the Flex-LCC, the insulation design of the arm inductors of the FBMMC part deviates

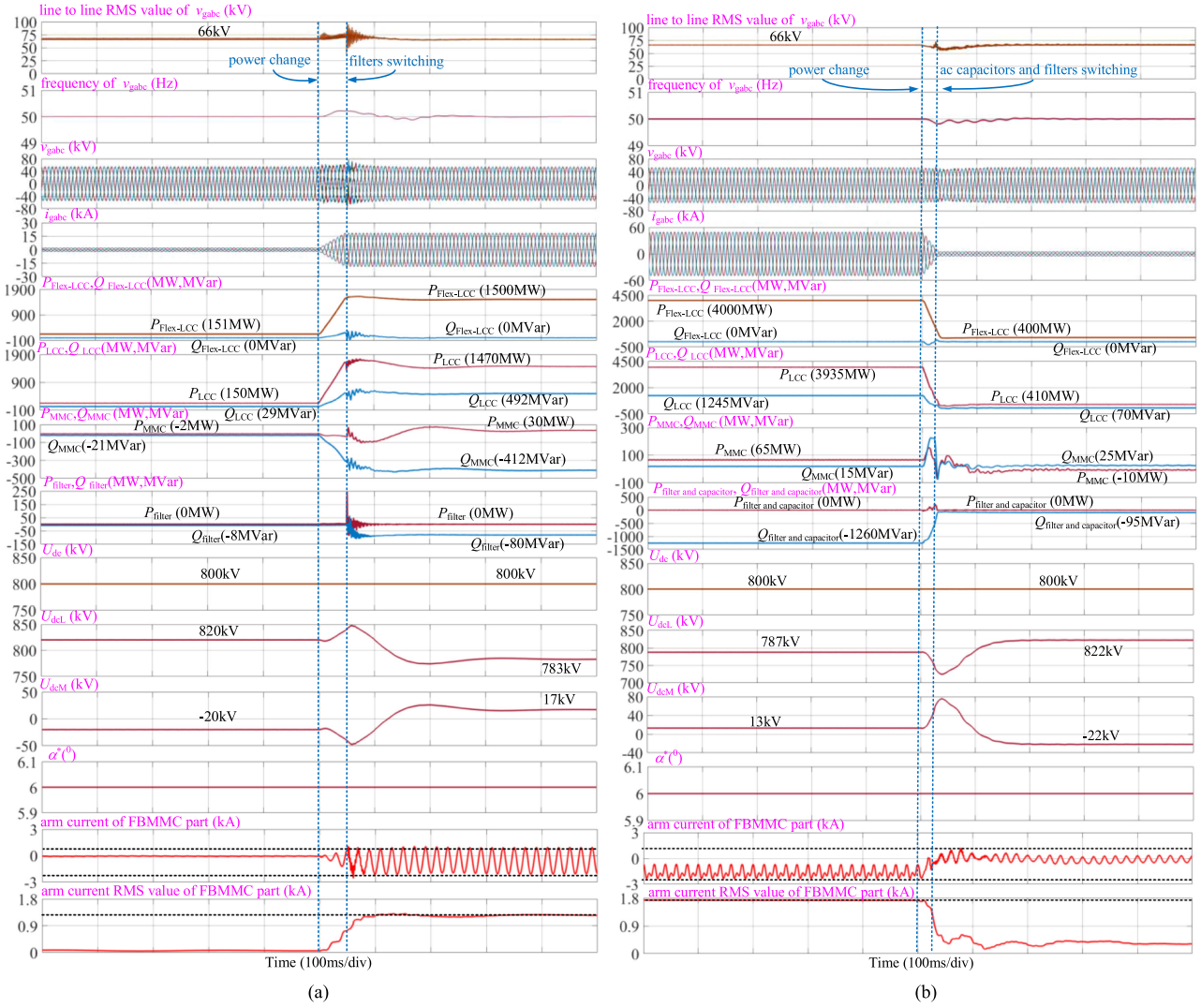

Fig. 5. Simulation results of the Flex-LCC. (a) Case I. (b) Case II.

from that of a conventional FBMMC. This distinction arises due to the decoupling of the dc-port voltage and the capacitor voltage of the FBMMC part in the Flex-LCC. Consequently, the transient overvoltage of U_{dcM} directly influences the voltage of the arm inductor instead of the submodule capacitor. Hence, in practical applications, careful consideration of the impact of U_{dcM}'s transient overvoltage on the insulation design of the arm inductor is necessary to ensure safe operation, particularly amidst dramatic power fluctuations in the Flex-LCC.

B. Experimental Results

To further validate the theory, a prototype with $q_{\mathrm{M}} = 1$ has been constructed, as illustrated in Fig. 6, and the main parameters of the Flex-LCC prototype are provided in Table II. In the experiment, the ac source simulator is connected to the Flex-LCC via a 6-Ω resistor, and the results are shown in Fig. 7.

In Fig. 7(a) and (b), the steady-state results of the Flex-LCC prototype under $U_{\mathrm{dc}} = 500$ V, $P_{\mathrm{Flex\text{-}LCCC}} = 2.6$ kW are presented. The peak value of the ac source line-to-line voltage

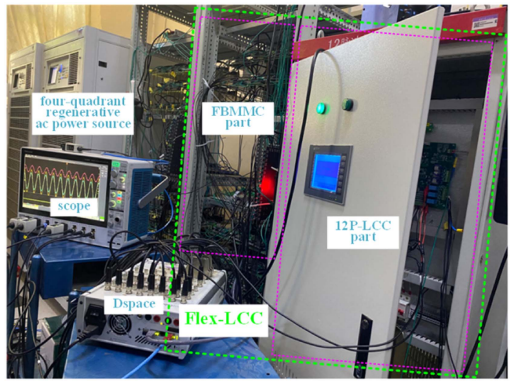

Fig. 6. Photograph of the Flex-LCC prototype.

is controlled at 394 V by a source simulator, and the peak value of the ac terminal line-to-line voltage of the Flex-LCC prototype is actively controlled at 283 V, verifying the ability of the Flex-LCC to control ac voltage. Meanwhile, the dc voltages

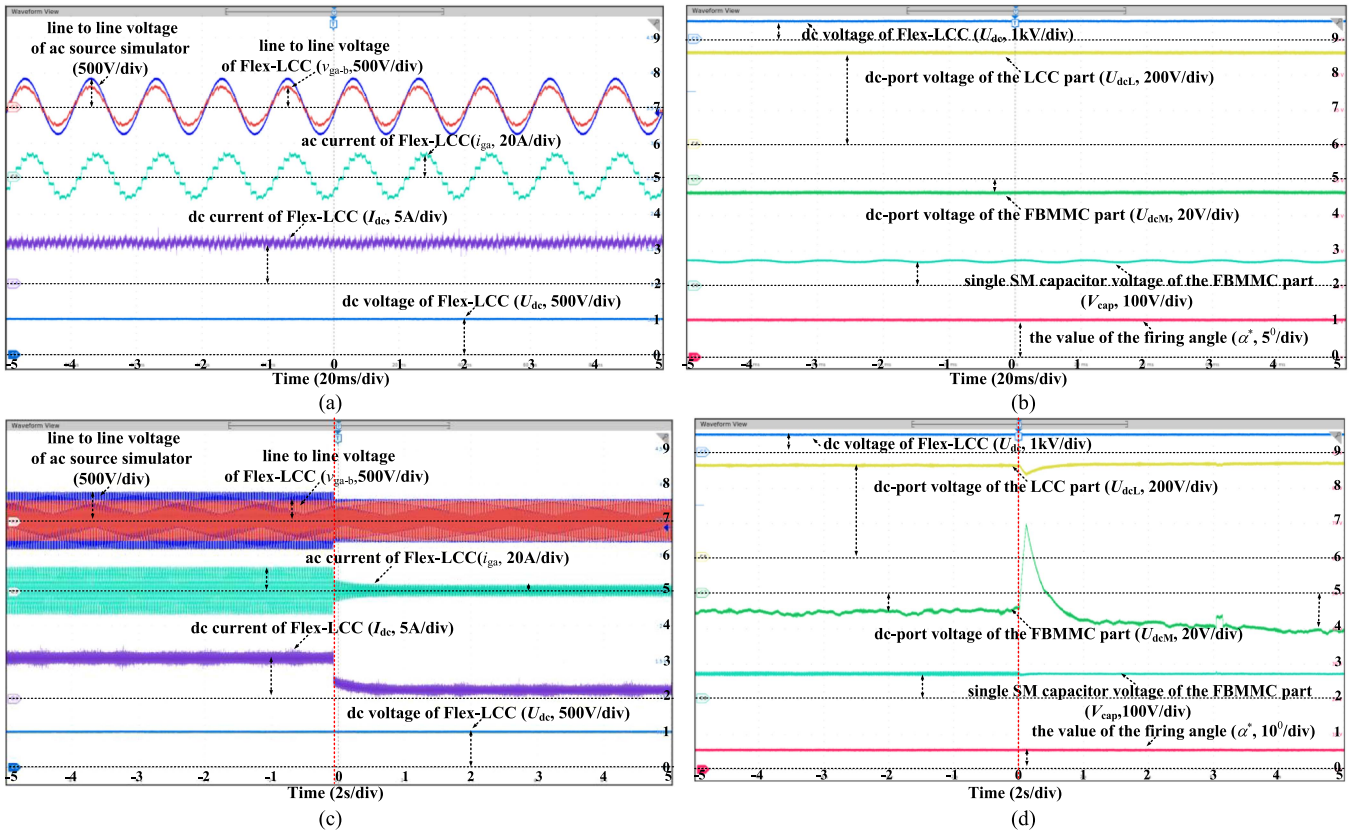

Fig. 7. Experimental results of the Flex-LCC. (a) Steady-state results, part I. (b) Steady-state results, part II. (c) Dynamic results, part I. (d) Dynamic results, part II.

TABLE II
MAIN PARAMETERS OF THE FLEX-LCC PROTOTYPE

Parameters	Value
$\sqrt{3/2}V_g$, ω_g	200 V, 50 Hz
U_{dc}, $P_{rFlex\text{-}LCC}$	500 V, 2600 W
α^*	5^0
Maximum reactive power of ac filters and ac capacitor banks	/
SM voltage	65 V
$V^*_{cap\Sigma}$	260 V
Number of SMs	4
Equivalent switching frequency	2000 Hz
k_L	1:1
k_M	/
Short-circuit ratio of the ac system in experimental verification	2.5

of the LCC and FBMMC part in the Flex-LCC are 510 and −10 V approximatively. That is, the FBMMC part only transmits about −52 W (2%) active power when the active power of the Flex-LCC is 2600 W, and the ac phase voltage amplitude (163 V) of the FBMMC is obviously larger than 0.5 times of its dc voltage (−10 V). In addition, the SM capacitor voltage is 65 V (the sum of capacitor voltages per arm is $65 \times 4 = 260$ V) when the dc-port voltage of the FBMMC is −10 V, verifying the decoupling of dc-port voltage and the capacitor voltage in the FBMMC part of the Flex-LCC. Fig. 7(b) also shows the firing angle of the LCC part is fixed at 5° and there is no fluctuation. These all show that the discussed salient features of the Flex-LCC are correct.

In Fig. 7(c) and (d), the dynamic results (ac source voltage is changed from 394 to 294 V and power is changed from 2.6 to 0.4 kW) of the Flex-LCC are presented. Obviously, the internal dc voltage ratio of the Flex-LCC is varied and distributed adaptively with the change of power. For example, when $P_{\text{Flex-LCC}} = 2.6$ kW, $U_{\text{dcL}} = 510$ V, and $U_{\text{dcM}} = -10$ V; when $P_{\text{Flex-LCC}} = 0.4$ kW, $U_{\text{dcL}} = 525$ V, and $U_{\text{dcM}} = -25$ V. This characteristic is obviously different with a conventional SCH valve. Meanwhile, the firing angle of the LCC part is always fixed at 5° and has no change when the power of the Flex-LCC changes from 2.6 to 0.4 kW, verifying the correctness of the theory analysis again.

VI. CONCLUSION

Using a novel control scheme of the SCH valve based on the LCC and FBMMC, a novel grid-forming HVdc rectifier, Flex-LCC, was proposed in this article for collecting large-scale islanded or weak-grid-supported RESs. The characteristics of the Flex-LCC allowed it to facilitate the matching of current-carrying capacity between the LCC and FBMMC and optimize the cost, footprint, and weight of the whole SCH valve. Typically, by using the proposed design, the rated dc voltage and active power for the FBMMC part both can be

designed within 10% of the Flex-LCC when the reactive power capacity of the FBMMC can be designed flexibly according to different demands. Meanwhile, the control-link fluctuation of the LCC part was eliminated, reducing the interharmonic pollution and enhancing the stability of the Flex-LCC. In addition, Flex-LCC can be used to shape diverse techno-economic grid-forming HVdc rectifier through reasonable designs. For instance, the designed 1500-MW, ±400-kV OWF converter station and 4000-MW, 800-kV onshore UHVdc station in this article both highlighted the diverse applications of the Flex-LCC. In conclusion, when considering engineering applications and investment economics, the proposed Flex-LCC stands out as a highly effective and promising HVdc rectifier for integrating large-scale islanded or weak-grid-supported RESs into power grids. This effectiveness was rooted in the mature technology used in the power circuit of Flex-LCC, which included only LCC and FBMMC parts, avoiding the use of less mature power electronic circuit structures.

REFERENCES

[1] M. Barns, D. Van Hertem, S. P. Teeuwsen, and M. Callavik, "HVDC systems in smart grids," *Proc. IEEE*, vol. 105, no. 11, pp. 2082–2098, Nov. 2017.

[2] D. Van Hertem et al., "Substations for future HVDC grids: Equipment and configurations for connection of HVDC network elements," *IEEE Power Energy Mag.*, vol. 17, no. 4, pp. 56–66, Jul./Aug. 2019.

[3] Y. Xue, X.-P. Zhang, and C. Yang, "Series capacitor compensated AC filterless flexible LCC HVDC with enhanced power transfer under unbalanced faults," *IEEE Trans. Power Syst.*, vol. 34, no. 4, pp. 3069–3080, Jul. 2019.

[4] T. Zuo, Y. Zhang, K. Meng, Z. Tong, Z. Y. Dong, and Y. Fu, "A two-layer hybrid optimization approach for large-scale offshore wind farm collector system planning," *IEEE Trans. Ind. Inform.*, vol. 17, no. 11, pp. 7433–7444, Nov. 2021.

[5] J. Hu, M. Xiang, L. Lin, M. Lu, J. Zhu, and Z. He, "Improved design and control of FBSM MMC with boosted ac voltage and reduced DC capacitance," *IEEE Trans. Ind. Electron.*, vol. 65, no. 3, pp. 1919–1930, Mar. 2018.

[6] M. Changizian, A. Mizani, and A. Shoulaie, "Proposed a new voltage rebalancing method for pole-to-ground fault in bipolar two-level VSC-HVDC," *IEEE Trans. Ind. Electron.*, vol. 69, no. 3, pp. 2157–2165, Mar. 2022.

[7] M. B. Ghat, S. K. Patro, and A. Shukla, "The hybrid-legs bridge converter: A flexible and compact VSC-HVDC topology," *IEEE Trans. Power Electron.*, vol. 36, no. 3, pp. 2808–2822, Mar. 2021.

[8] W. Xiang, S. Yang, G. P. Adam, H. Zhang, W. Zuo, and J. Wen, "DC fault protection algorithms of MMC HVDC grids: Fault analysis, methodologies, experimental validations and future trends," *IEEE Trans. Power Electron.*, vol. 36, no. 10, pp. 11245–11264, Oct. 2021.

[9] K. Sun, H. Xiao, J. Pan, and Y. Liu, "A station-hybrid HVDC system structure and control strategies for cross-seam power transmission," *IEEE Trans. Power Syst.*, vol. 36, no. 1, pp. 379–388, Jan. 2021.

[10] P. Bakas et al., "A review of hybrid topologies combining line-commutated and cascaded full-bridge converters," *IEEE Trans. Power Electron.*, vol. 32, no. 10, pp. 7435–7448, Oct. 2017.

[11] H. Jiang and A. Ekstrom, "Harmonic cancellation of a hybrid converter," *IEEE Trans. Power Del.*, vol. 13, no. 4, pp. 1291–1296, Oct. 1998.

[12] Z. Xu et al., "Hybrid high-voltage direct current topology with line commutated converter and modular multilevel converter in series connection suitable for bulk power overhead line transmission," *IET Power Electron.*, vol. 9, no. 12, pp. 2307–2317, Oct. 2016.

[13] P. Bakas et al., "Review of hybrid multilevel converter topologies utilizing thyristors for HVDC applications," *IEEE Trans. Power Electron.*, vol. 36, no. 1, pp. 174–190, Jan. 2021.

[14] P. Meng, W. Xiang, Y. Chi, Z. Wang, W. Lin, and J. Wen, "Resilient DC voltage control for islanded wind farms integration using cascaded hybrid HVDC system," *IEEE Trans. Power Syst.*, vol. 37, no. 2, pp. 1054–1066, Feb. 2021.

[15] C. Niu, M. Yang, R. Xue, L. Zhu, X. Wang, and J. Wu, "Research on inverter side AC fault Ride-through strategy for hybrid cascaded multi-terminal HVDC system," in *Proc. IEEE 4th Conf. Energy Internet Energy Syst . Integration*, 2020, pp. 800–805.

[16] H. Huang, J. Ma, S. Wang, Y. Dong, N. Jiao, and T. Liu, "Accurate analysis of harmonic transmission of line commutated converter considering firing angle fluctuation," *IEEE Access*, vol. 8, pp. 205206–205215, 2020.

[17] H. Xiao et al., "Review of hybrid HVDC systems combining line communicated converter and voltage source converter," *Int. J. Elect. Power Energy Syst.*, vol. 129, pp. 1–9, Jul. 2021.

[18] S. Debnath, J. Qin, B. Bahrani, M. Saeedifard, and P. Barbosa, "Operation, control, and applications of the modular multilevel converter: A review," *IEEE Trans. Power Electron.*, vol. 30, no. 1, pp. 37–53, Jan. 2015.

[19] Z. Liu and J. Zhao, "Disturbance interaction analysis and suppression strategy of MMC-HVDC systems considering sub-module capacitor voltage ripples," *IEEE Trans. Power Syst.*, vol. 36, no. 1, pp. 235–247, Jan. 2021.

[20] R. Blasco-Gimenez, N. Aparicio, S. Ano-Villalba, and S. Bernal-Perez, "LCC-HVDC connection of offshore wind farms with reduced filter banks," *IEEE Trans. Ind. Electron.*, vol. 60, no. 6, pp. 2372–2238, Jun. 2013.

[21] CIGRE Working Group B4.46, *Voltage Source Converter (VSC) HVDC For Power Transmission—Economic Aspects and Comparison With Other AC and DC Technologies, Technical Brochure*, CIGRE, Paris, France, Apr. 2012.

[22] A. Nami, J. L. R. Amenedo, S. Arnaltes, M. Á. Cardiel-Álvarez, and R. A. Baraciarte, "Frequency control of offshore wind farm with diode-rectifier-based HVDC connection," *IEEE Trans. Energy Convers.*, vol. 35, no. 1, pp. 130–138, Mar. 2020.

[23] N. Chen, K. Zha, H. Qu, F. Li, Y. Xue, and X.-P. Zhang, "Economic analysis of flexible LCC-HVDC systems with controllable capacitors," *CSEE J. Power Energy Syst.*, vol. 8, no. 6, pp. 1708–1719, Nov. 2022.

Qianhao Sun (Member, IEEE) was born in Shanxi, China, in 1993. He received the B.S. degree in electrical engineering from Northeast Electric Power University, Jilin, China, in 2014, and the M.S. and Ph.D. degrees in electrical engineering from Tsinghua University, Beijing, China, in 2017 and 2020, respectively.

From May to November, 2019, he was a visiting Ph.D. student with Cardiff University, Cardiff, U.K. He is currently a Postdoctoral Fellow with Tsinghua University. His current research interests include flexible ac and dc transmission and distribution system, renewable energy generation, high-power electronic interfaces for utility system, and dc–dc converter.

Qiang Song (Senior Member, IEEE) was born in Changchun, China, in 1975. He received the B.E.E. and Ph.D. degrees in electrical engineering from Tsinghua University, Beijing, China, in 1998 and 2003, respectively.

From 2003 to 2008, he was a Lecturer with the Department of Electrical Engineering, Tsinghua University, where since 2008, he has been an Associate Professor. His main research interests include high power electronic interfaces for utility system, flexible ac transmission system, voltage-source converter-HVdc system, and custom power quality.

Jingwei Meng was born in Liaoning, China, in 1990. He received the B.S. degree in electrical engineering, in 2015, from the Department of Electrical Engineering, Tianjin University, Tianjin, China, and the M.S. degree in electrical engineering, in 2018, from the Department of Electrical Engineering, Tsinghua University, Beijing, China, where he is currently working toward the Ph.D. degree in electrical engineering.

His current research interest includes voltage-source-converter-HVdc system.

Bin Cui (Member, IEEE) received the B.S. degree in electrical engineering from the Harbin Institute of Technology, Harbin, China, in 2009, the M.S. degree in electrical engineering from Fuzhou University, Fuzhou, China, in 2012, and the Ph.D. degree in electrical engineering from the Department of Electrical Engineering, Tsinghua University, Beijing, China, in 2019.

He is currently a Postdoctoral Fellow with Tsinghua University. His research interest includes high-frequency dc–dc converters, and flexible dc system.

Gen Li (Senior Member, IEEE) received the B.Eng. degree in electrical engineering from Northeast Electric Power University, Jilin, China, in 2011, the M.Sc. degree in power engineering from Nanyang Technological University, Singapore, in 2013, and the Ph.D. degree in electrical engineering from Cardiff University, Cardiff, U.K., in 2018.

From 2013 to 2016, he was a Marie Curie Early Stage Research Fellow funded by the European Commission's MEDOW project. He was a Research Associate with the School of Engineering, Cardiff University, from 2018 to 2022. He is currently an Associate Professor with the Technical University of Denmark (DTU), Kongens Lyngby, Denmark.

Dr. Li was the recipient of the First CIGRE Thesis Award in 2018 for his Ph.D. thesis. He is a Chartered Engineer in the U.K., a Young Editorial Board Member of *Applied Energy*, an Associate Editor for *CSEE Journal of Power and Energy Systems* and *IET Energy Systems Integration*, an Editorial Board Member of *CIGRE ELECTRA* and *Global Energy Interconnection* and an IET Professional Registration Advisor.

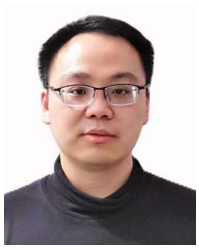

Fan Cheng received the B.S. degree in electrical engineering and automation from the South China University of Technology, Guangzhou, China, in 2014, the M.Eng. degree in electrical engineering from Southeast University, Nanjing, China, in 2010, and the Ph.Eng. degree in electrical engineering from China Electric Power Research Institute, Beijing, China, in 2021.

He is currently a Postdoctoral Researcher with the Center for Strategic Studies, Chinese Academy of Engineering. His research interest includes large-scale renewable energy integration, and renewable energy development planning.

Kailun Wang was born in Henan, China, in 1998. He received the B.E. degree in electrical engineering in 2020 from Tsinghua University, Beijing, China, where he is currently working toward the Ph.D. degree in electrical engineering with the Department of Electrical Engineering.

His current research interest includes voltage-source-converter-HVdc and modular multilevel converter